Novel Coil Array Design and Modeling for Independent Control of Multiple Magnetic Microrobots

Guangming Cui, Pengsong Zhang, Xinyu Liu, *Member IEEE*, Linbo Xie, Wentao Huang, Peng Pan, Juntian Qu, *Member IEEE*, and Qigao Fan, *Member IEEE*

***Abstract*—The independent control of microrobot swarms is a major challenge in the field of micro/nano manipulation. In this paper, a new localized magnetic field generating system is presented that can be used for the independent control of multiple magnetic microrobots. Such a system will allow for cooperative or parallel microassembly tasks with teams of magnetic microrobots. Firstly, the performance of the novel circular microcoil is modeled by analyzing the effect of input current to study the magnetic field distribution characteristics in the workspace, which is validated by finite element analysis and simulation; then, an actuation and control strategy of microrobots for microcoil array is proposed. Meanwhile, the independent closed-loop control of the microrobot is realized based on visual feedback; finally, an experimental platform for the microcoil actuation system is built to validate the newly designed structure. The results show that the microrobot can move flexibly and accurately with the tracking error within 0.444mm. At the same time, the system is capable of independently controlling multiple microrobots and holds great potential in performing micromanipulation tasks.**

***Index Terms*—Magnetic field actuation, microrobots, independent control.**

I. Introduction

IN RECENT years, micro/nanorobots have drawn a lot of interest in the area of robotics because they have great potential to enhance the functionality of micromanipulation in biological, medical, chemical, and industrial environments. Being small and untethered, independent control of teams and swarms of such microrobots can be used for parallel and collaborative tasks at micro-scale, such as targeted drug delivery, bioassay, micro parts separation, assembly, manipulation, and chemical analysis [1]-[5].

One of the main challenges in designing such microrobots is in ensuring sufficient power supply from external because it is difficult to mount conventional power sources on the microrobots. In the past decade, there have been several solutions to design and develop such microrobots using optical energy, acoustic energy, thermal energy, biological energy, magnetic fields, and physiological energy [6]-[9]. Electromagnetic actuation has provided promising results to date [10]-[18] because of its ability to penetrate most materials, suitability to actuate objects remotely, and security to humans. For such actuation systems, the microrobots are usually made of permanent magnetic or paramagnetic materials that respond to the magnetic field generated by external electromagnetic coils. Therefore, microrobots can be controlled by changing the magnitude and direction of the currents through electro-magnetic coils. However, due to the interaction between microrobots and magnetic field generated by such coils, multiple microrobots will respond to the global magnetic field simultaneously when they are present in the workspace, which results in restricting independent control to a single microrobot at a time.

Recently, using a global magnetic field to actuate multiple microrobots independently has attracted people's attention [19], [20]. The difference in shape or magnetic properties of magnetic microrobots was exploited to obtain independent control of microrobots using a global magnetic field [21], [22]. Especially in [23], a pair of identical and nonidentical microrobots were independently controlled in the 3D space by exploiting the inhomogeneity of the strong fields the system can generate. While the nonuniformity of the microrobots' magnetic properties and the inhomogeneity of the strong fields allowed them to behave differently when exposed to the same magnetic field, their motions were still coupled, and hence, this approach cannot be extended to deal with large numbers of microrobots. Thus, to overcome the challenge of using a single global magnetic field for multi-robot control, some local

Manuscript received January 22, 2022; revised June 24, 2022 and September 1, 2022; accepted November 8, 2022. This work was supported in part by the Six Talent Peaks Project in Jiangsu Province under Grant GDZB-138, in part by the 111 Project under Grant B12018, in part by the China Postdoctoral Science Foundation 2020M681749, and in part by the Natural Science Foundation of Jiangsu Province under Grant BK20210475. *(Corresponding author: Qigao Fan.)*

G. Cui, P. Zhang, L. Xie, W. Huang, and Q. Fan are with the School of Internet of Things Engineering, Jiangnan University, Wuxi 214122, China (e-mail: gmingcui@126.com; pengsongzhang@126.com; xie_linbo@jiangnan.edu.cn; wentao.h@jiangnan.edu.cn; qgfan@jiangnan.edu.cn).

X. Liu and P. Pan are with the Department of Mechanical and Industrial Engineering, University of Toronto, Toronto M5S 3G8, Canada (e-mail: xyliu@mie.utoronto.ca; peng.pan@mail.utoronto.ca).

J. Qu is with the Department of Mechanical Engineering, Tsinghua University, Beijing 100084, China (e-mail: juntianqu@mail.tsinghua.edu.cn).

magnetic fields were used instead. Two kinds of microcoil array structures are generally adopted to generate local magnetic field. Micro-wire strips [24], [25] are arranged orthogonally in two layers to generate sufficient force in two planar axes. In this structure, microrobots are actuated through the activation of specific microcoil arranged in the X or Y direction. However, the workspace of this method is relatively small, and expanding the workspace may complicate the design of driving circuit. So it restricts the presence of multiple microrobots in the workspace simultaneously. The square spiral coil structure [26], [27] directly utilizes attractive field and repulsive field to drive microrobots. Although this structure has a larger workspace that allows for the presence of multiple microrobots, how to realize precise and flexible control of microrobots is still a challenge, particularly when performing micromanipulation tasks.

In this article, a local magnetic field generating system consisting of an 8×8 planar circular spiral microcoil array is developed to independently actuate multiple microrobots. The shape of microcoil is optimized to produce a uniformly distributed magnetic field. The theoretical analysis indicates that using a circular spiral structure can generate a uniformly distributed magnetic field along the circumference. The successful transportation of multiple microrobots between any equilibrium points with the tracking error within 0.444mm by using the designed coil array actuation system has efficiently demonstrated the effectiveness of the proposed design approach for micromanipulation applications.

The main contribution of this article is to design a novel local magnetic field generating system consisting of an 8×8 planar circular spiral microcoil array with three layers, which lies in magnetic field uniform distribution and accurate and flexible control of the microrobot. The micro-wire strips array system with a workspace of 13 ×17 mm can achieve the control of one robot [25]. It is difficult to control one more robot in such a small workspace at the same time due to the magnetic interaction of microrobots. The square spiral microcoil array system [27] allows for the controlling of four robots at most. However, the magnetic field generated by the square coil is only distributed in four directions, which may restrict the flexible and precise control of the microrobots. In comparison to previous works, the actuation system reported in this article can generate a series of local magnetic fields evenly distributed along the circumference, which render the actuation of microrobots flexible and precise.

The remaining part of this article is structured as follows: Section II introduces the design and modeling of the circular microcoil array system. Section III introduces the hardware and software platform, including the strategy of actuation and control for microrobots. Section IV provides experimental demonstrations of the developed microcoil platform. Finally, Section V concludes this article.

II. Microcoil Design and Modeling

This section discusses how to design microcoil array to generate a number of local magnetic fields. To improve the actuation capability of microrobots, a three-layer planar circular spiral coil is designed. In addition, the equivalent model of microcoil is established and verified by finite element model.

A. Circular Microcoil Array Design

To generate a series of discrete local magnetic fields to independently actuate multiple microrobots, an 8 × 8 planar circular spiral microcoil array which contains 64 microcoils with a diameter of 3 mm was designed and developed, as shown in Fig. 1. The microcoils were designed with three layers to enhance the generated magnetic fields, each layer has 5 turns, the winding width was set to 0.15 mm and the spacing between the windings was 0.1 mm. Each microcoil was individually connected to a power source. These microcoils can provide magnetic actuation forces around them when the currents are supplied. By changing the magnitude and direction of the current, the motion of the microrobot will be controlled.

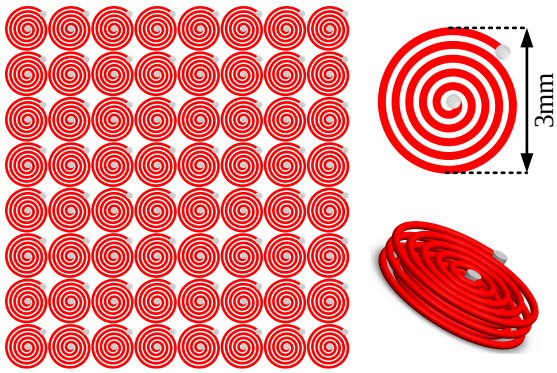

Fig. 1. Schematic showing how the three-layer coils are arranged in the workspace.

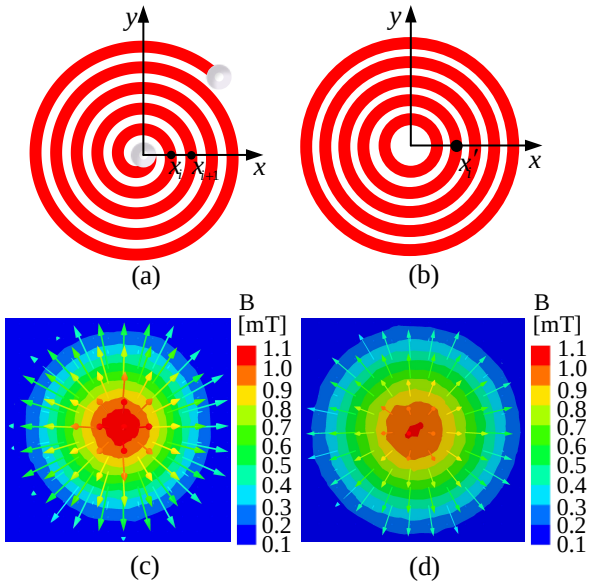

Fig. 2. Microcoil equivalent model and field distributions. (a) Planar circular spiral coil and (b) its equivalent concentric-loop model. (c) and (d) Planar circular spiral coil and multiple-loop coils magnetic flux density distribution.

B. Magnetic Force Model

The magnetic field is first studied for researching magnetic force generated by the microcoils, to obtain its distribution characteristics. The current traces are connected to the

microcoils through vias and they are separated from the microcoils through an insulation layer. For the analytical study, it is assumed that these vias and current traces have no influence on the magnetic field in the workspace.

For closely spaced turns, the multiturn planar spiral is generally approximated as some concentric loops with various radii to study its magnetic field characteristics [28]. As illustrated in Fig. 2(a) and (b), a circular spiral coil is equivalent to multiple concentric current loops without interconnects between loops. The radius of the *i*th loop is given by

$$x_i' = \frac{x_i + x_{i+1}}{2} \tag{1}$$

where x_i and x_{i+1} are the minimal and maximal distance of the *i*th turn away from the center of the coil.

It is assumed that the currents in all loops are equal and unidirectional, then the multiloop model provides a close approximation of the circular spiral coil for a fast calculation of the magnetic field. The two different structures were simulated with ANSYS Maxwell. As shown in Fig. 2(c) and (d), the vector distribution characteristics of the magnetic induction intensity for the two structures are the same when 0.75 A current is applied. They all point from the center of the coil to the outside of the circle in the radial direction, and the magnetic induction intensity reaches the peak value at the center of the coil.

To establish an analytical model, the magnetic field generated by a single loop is evaluated first, then superpose the magnetic fields generated by these single loops to calculate the magnetic field of multiple loops, and finally, the field distribution of the three-layer coil is available. According to the Biot–Savart law, the magnetic induction intensity of a single loop shown in Fig. 3 is given by

$$\boldsymbol{B} = \frac{\mu_0}{4\pi}\int_C \frac{I d\boldsymbol{l} \times \boldsymbol{r}'}{|\boldsymbol{r}'|^3} \tag{2}$$

where C represents the loop with a radius of x_i', I is the amplitude of the current flowing in the loop, $\boldsymbol{r}'$ is the displacement vector between the current element $Id\boldsymbol{l}$ and any point $p(x_0, y_0, z_0)$ in space, and μ_0 is the space permeability.

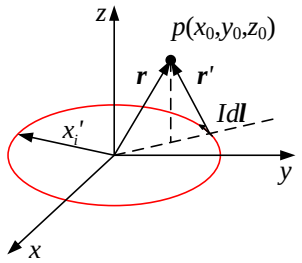

Fig. 3. Calculation of magnetic field for a single loop. The magnetic field at point $p(x_0, y_0, z_0)$ is calculated by integrating the current element $Id\boldsymbol{l}$ along the loop.

To simplify the calculation, the components of the magnetic flux density along the X-axis, Y-axis, and Z-axis are respectively calculated, which is given by

$$B_{xji}(x_0, y_0, z_0) = \frac{\mu_0 I}{4\pi}\int_C \frac{(z_0 - z)}{r'^3} dy - \frac{(y_0 - y)}{r'^3} dz \tag{3}$$

$$B_{yji}(x_0, y_0, z_0) = \frac{\mu_0 I}{4\pi}\int_C \frac{(x_0 - x)}{r'^3} dz - \frac{(z_0 - z)}{r'^3} dx \tag{4}$$

$$B_{zji}(x_0, y_0, z_0) = \frac{\mu_0 I}{4\pi}\int_C \frac{(y_0 - y)}{r'^3} dx - \frac{(x_0 - x)}{r'^3} dy \tag{5}$$

where *i* represents the loop, and *j* represents the layer.

Then, the magnetic flux density at point $p(x_0, y_0, z_0)$ generated by three-layer concentric rings can be calculated by

$$B_x = \sum_{j=1}^{3}\sum_{i=1}^{5} B_{xji}(x_0, y_0, z_0) \tag{6}$$

$$B_y = \sum_{j=1}^{3}\sum_{i=1}^{5} B_{yji}(x_0, y_0, z_0) \tag{7}$$

$$B_z = \sum_{j=1}^{3}\sum_{i=1}^{5} B_{zji}(x_0, y_0, z_0) \tag{8}$$

The magnetic field generated by the microcoil along the Y-axis at a height $z = 0.5$ mm is calculated using the equations above when 0.75 A current is applied to the microcoil. A FEM model was also designed in ANSYS Maxwell, considering the thickness of the microcoil to verify the analytical model. The comparison results of the analytical model and FEM model are shown in Fig. 4(a). It is easily seen that the analytical model can accurately estimate the spatial magnetic field.

Considering the symmetry and uniformity of the magnetic field generated by the microcoil, the magnetic field gradient in the whole workspace can be obtained as long as the distribution of the magnetic field gradient along one direction is known. Differentiate B_y and B_z along the y-direction and z-direction respectively, the magnetic field gradient distributions along the Y-axis at a height z = 0.5 mm are shown in Fig. 4(b). Due to the magnetic field $\boldsymbol{B}(x, y, z)$, the magnetic force $\boldsymbol{F}_{mag}$ on microrobot is a function of the magnetic field gradients and can be calculated as

$$\boldsymbol{F}_{mag} = V_r(\boldsymbol{M}.\nabla)\boldsymbol{B}(x, y, z) \tag{9}$$

where V_r is the volume of the microrobot, $\boldsymbol{M}$ is the magnetization of the magnetic microrobot, and $\boldsymbol{B}(B_x, B_y, B_z)$ is the magnetic flux density produced by the microcoils.

For microrobots magnetized along the thickness direction, $\boldsymbol{M}(M_x, M_y, M_z)$ is approximate to M_z, so the magnetic force can be simplified as

$$F_{mag} = V_r M_z\left(\frac{\delta B_x}{\delta z}a_x + \frac{\delta B_y}{\delta z}a_y + \frac{\delta B_z}{\delta z}a_z\right) \tag{10}$$

The calculated magnetic force along the Y-axis at the plane z = 0.5 mm is shown in Fig. 4(c). And then the dynamic equation of the microrobot under the influence of magnetic force $\boldsymbol{F}_{\text{mag}}$ can be described as

$$\boldsymbol{F}_{mag} + \boldsymbol{F}_{fric} + \boldsymbol{F}_{drag} = m\ddot{s} \tag{11}$$

where *m* represents the mass of the microrobot, *s* is the position of the microrobot, F_{fric} is the friction of the microrobot in the workspace, and F_{drag} is the drag force generated by fluid, respectively.

III. Microrobot Actuation and Control

This section presents the hardware for independent microrobot control consisting of the six-layer microcoil platform, the coil current drive electronics, and a CCD camera,

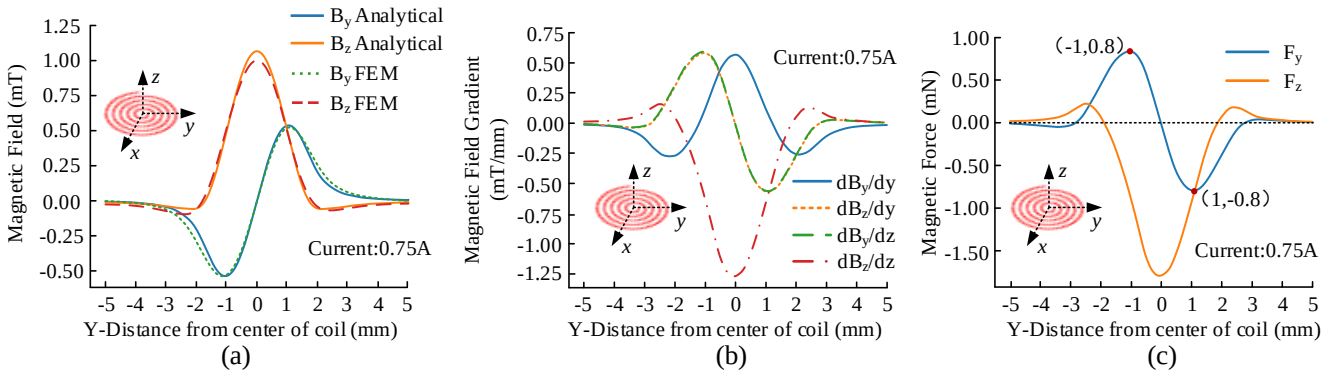

Fig. 4. Calculation of fields generated by the microcoil. (a) Magnetic field along the Y-axis at the plane z = 0.5 mm calculated by the analytical model and FEM with current: 0.75 A. (b) Magnetic field gradients along the Y-axis at the plane z = 0.5 mm due to a microcoil carrying 0.75 A current. Differentiate B_y and B_z along the y-direction and z-direction, respectively. (c) Magnetic force along the Y-axis at the plane z = 0.5 mm generated by a microcoil carrying 0.75 A current for an N52 disc magnet microrobot with magnetization along the Z direction (2.5 mm diameter, 0.5 mm thick).

as shown in Fig. 5(a). Based on the visual feedback, the actuation and control strategy of the microrobot between equilibrium points is proposed. Furthermore, the custom software that outputs the currents at the microcoils required for actuation according to the received position of the microrobot and desired trajectory is also introduced.

A. Microcoil Platform

The microcoil platform shown in Fig. 5(c) which was fabricated with standard PCB technology consists of the PCB with 64 circular spiral microcoils. The PCB contains a 27 × 27 mm workspace with a total of 6 layers where the top three layers form the microcoils and the bottom three layers form the required connections to the control electronics. This layout was designed to minimize the effect of current traces on the magnetic field in the workspace. The microcoils in the workspace have vias and current traces that lead to a set of jumper pins in the PCB and then are connected to the microcoil current driver circuits. To observe the microrobot moving in the workspace, a CCD camera is mounted above the workspace.

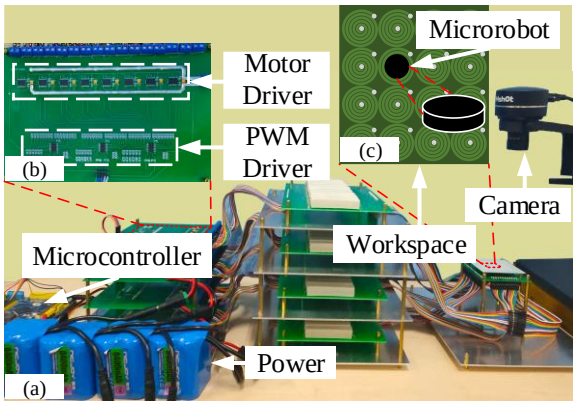

Fig. 5. Experimental platform. (a) Overview of the hardware platform consists of the microcontroller, the current control board, the workspace, and the camera for independent microrobot actuation. (b) Current control board. The PWM drivers and Motor drivers control the magnitude and direction of the current. (c) Part workspace view from the camera.

B. Current Control Electronics

The currents in the microcoils are output by the individual motor drivers (TB6612fng) for each microcoil. There are two H-bridge circuits in each motor drive chip so that the direction of the currents can be controlled by the conduction of different bridge arms. The PWM driver board (PCA9685) is used to control the intensity of the output currents. Each current control board can control up to 16 microcoils as shown in Fig. 5(b). Therefore, four controller boards are used to control the 64 microcoils. Each PWM board has custom preset addresses that are accessible through an I^2C interface, which allows for the control of the entire hardware platform with just two wires. These current control boards are designed by the circuit design tool (ALTIUM DESIGNER 20, Altium Inc., Australia). All the computation is performed on a desktop computer (Intel Core i5-10300H CPU, 16 GB RAM, 2.5 GHz), and commands are sent to the controller boards through an MCU (STM32-F103ZET6, 72 MHz, STMicroelectronics Inc., Switzerland). Four power supplies are used to provide power to all 64 microcoils, and each microcoil can continuously output current up to 1 A at the same time.

C. Microrobot Actuation

The magnetic force experienced by the microrobot with the currents in different directions is shown in Fig. 6(a) and (b). When the current is counterclockwise, the microrobot experiences an attractive force inside the coil to force it to move to the center of the coil, and a repulsive force outside the coil to keep it away from the coil. The force on microrobot is opposite when the current is clockwise. The direction of the force is always along the connecting line between the center of the microrobot and the coil. Fig. 6(c) shows the local magnetic field range when 0.5A current is applied.

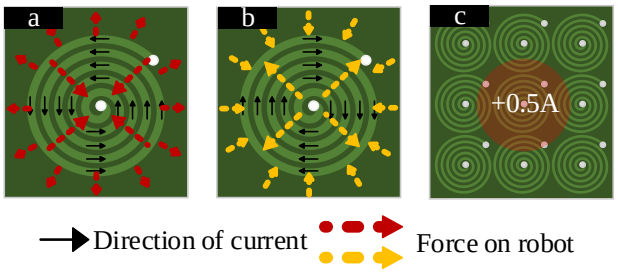

Fig. 6. Magnetic field effect when current is applied to a single coil. (a) Force on microrobot when counterclockwise current is applied. (b) Force on microrobot when clockwise current is applied. (c) Local magnetic field when 0.5A current is applied.

Based on analysis of the magnetic force of a single coil, there are two kinds of static equilibrium points defined in the workspace, one is the center of the microcoil when attracting the microrobot (a counterclockwise current is applied to the microcoil), which is defined as the central equilibrium point; the other is the midpoint of the common diagonal of any four coils when repulsing the microrobot (a clockwise current is applied to the microcoil), which is defined as the diagonal equilibrium point. There are eight motion forms for the microrobot at each equilibrium point which means it can move in eight directions. To actuate the microrobot to move along the desired trajectory, it is necessary to control multiple microcoils around the microrobot at the same time. The various motion states of the microrobot shown in Fig. 7(a)-(c) illustrate the actuation method of the microrobot moving between central equilibrium points, central equilibrium and diagonal equilibrium point, and diagonal equilibrium points. When the microrobot is in the center of the microcoil, this microcoil will exert no force on the microrobot, so it is necessary to activate surrounding microcoils to actuate the microrobot. However, the force generated by this microcoil will be dominant when the microrobot deviates from the center of the microcoil.

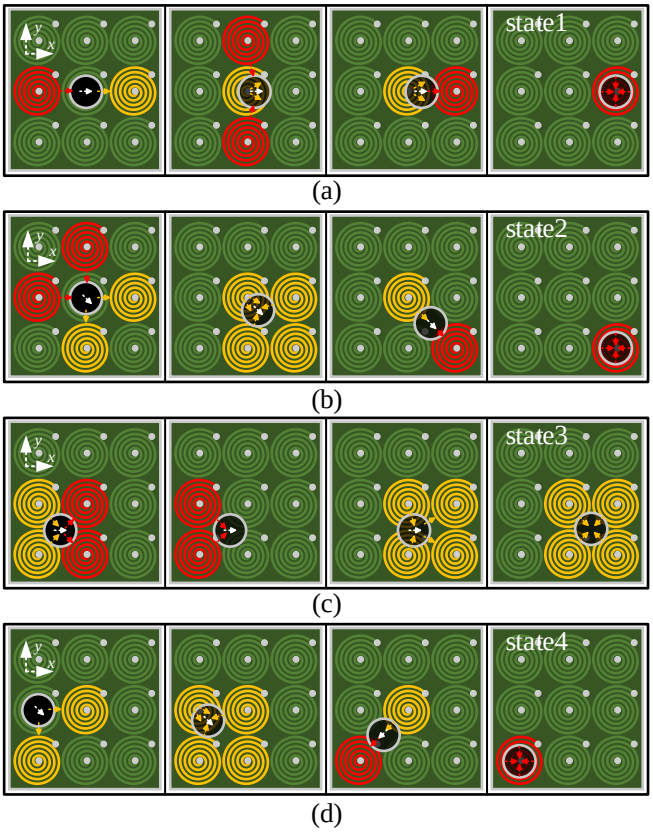

Fig. 7. Movement of the microrobot in the workspace due to specified microcoil activation. (a) Movement between central equilibrium points. (b) Movement between central equilibrium point and diagonal equilibrium point. (c) Movement between diagonal equilibrium points. (d) Movement at the edge of the workspace. (The yellow coil and red coil indicate that a clockwise and counterclockwise current is applied, respectively. Note that the red and yellow arrows indicate the force exerted by each coil, and the white arrows indicate the resultant force.)

The actuation of the microrobot at the edge of the workspace is also considered. Due to the reduction of microcoils available for actuation, the microrobot cannot move between central equilibrium points directly. As shown in Fig. 7(d), the microrobot moved to the diagonal equilibrium point first, and then moved to the target coil central equilibrium point, thereby achieving the movement between the edge microcoils.

D. Visual Feedback Control of Microrobot

During the movement of the microrobot, the position of the microrobot needs to be fed back in real-time, so as to activate microcoils around it and control the microrobot to move along the reference trajectory.

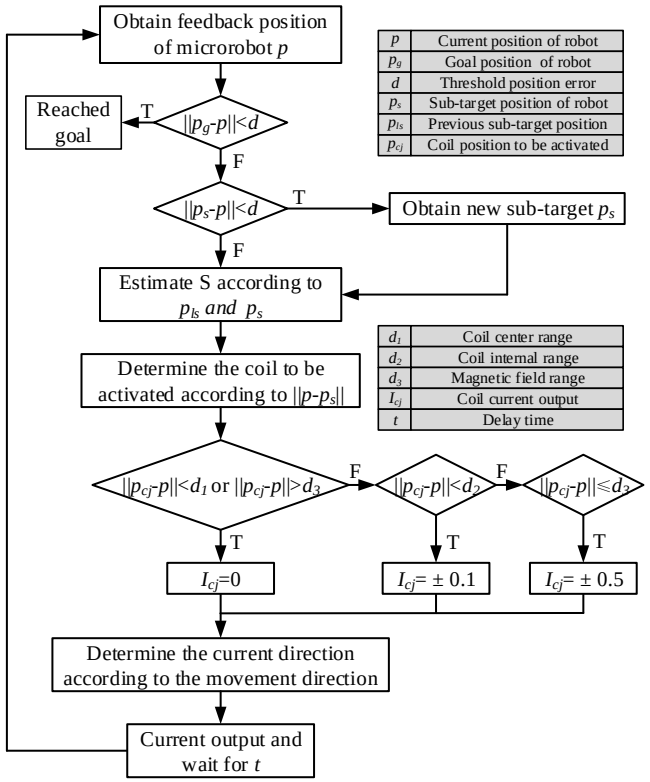

Fig. 8. Algorithm to determine the currents in the coils in the workspace. (Note that T and F are "True" and "False" respectively.)

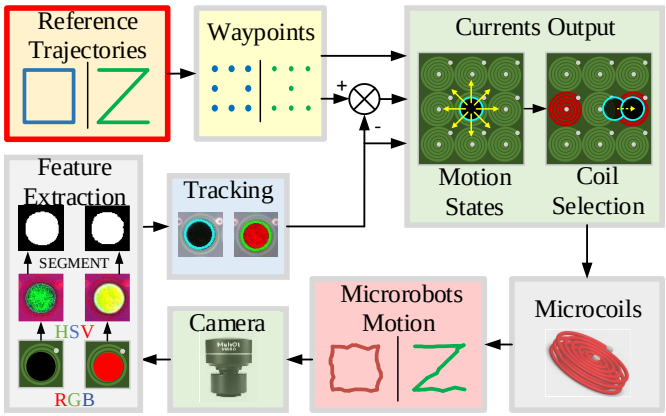

Fig. 9. Flowchart depicting the software structure of the developed device. For the purpose of tracking, the images captured by the camera are converted to hue-saturation-value (HSV) color space for better contrast among channels. In the process of tracking, the HSV image is then thresholded using experimentally determined values, and the contour detection algorithm is used to locate the microrobot.

The forces generated, however, are nonlinear due to the nature of the magnetic field. To simplify the control, therefore, the microcoil is divided into three areas: coil center, inside the coil, and outside the coil. Bang-bang controller is used to output currents required for actuation. The algorithm to estimate how the coil current output to move the robot from the current position, p, to p_g, is shown in Fig. 8. The flowchart of visual feedback control is shown in Fig. 9, the reference trajectory is discretized into a series of waypoints first, and then the state of the microrobot in the workspace is obtained through the camera. The motion state is determined and corresponding microcoils are selected according to the current position of the microrobot and the target position. Based on the error between microrobot and target position, the microcoils are activated with predefined currents with correct polarity to generate forces along the direction of the target position.

IV. Experiments and Analysis

The visual feedback control of the microrobots using the newly designed system is demonstrated here. The single-robot navigation experiment shows the capability of the microcoil platform to actuate the microrobot to move between any equilibrium points. In addition, the demonstration of curvilinear path is also carried out. The two-robot and three-robot navigation experiments illustrate the ability of the microcoil platform to independently control multiple microrobots in the workspace. Finally, the potential of this system to conduct assembly tasks has also been demonstrated.

A. Experimental Preparation

To reduce the frictional force experienced by the microrobot, silicone oil with 10 viscosity was added to the workspace. In the environment filled with silicone oil with 10 viscosity, the friction coefficient is approximately reduced to 0.1-0.2 [29]. Microrobots (N52 NdFeB disc magnets which are neodymium with nickel coating and are commercially available) with a diameter of 2.5 mm and a thickness of 0.5 mm used in the experiment, are magnetized along the thickness direction and their magnetic induction is 98.5 mT. These robots are oriented in the workspace with their north pole facing up to make sure that they will not attract together, which also ensures that they are under the same control. To keep track of the magnetization direction, the north pole of the robot is colored.

B. Single-Robot Navigation Experiment

In order to demonstrate the capabilities of the microcoil platform, the motion control experiment of a single microrobot was conducted first. The microrobot was actuated towards the user-defined waypoints in the workspace under the effect of local microcoils. Control laws prescribed combined with feedback information from the captured images were used to keep the microrobot moving along the desired trajectory. The feedback image was first used to calibrate the positions of the microcoils in the workspace, and then the position of the microrobot was measured through color threshold and localized through the contour detection algorithm.

The waypoints to define Z-shaped and square trajectories were chosen to showcase the different actuation capabilities of the microcoil platform at different static equilibrium points in the workspace. As shown in Fig. 10(a) and (b), the Z-shaped path along central equilibrium point and diagonal equilibrium point was successfully traversed autonomously. Since the magnetic force on the microrobot generated by the microcoils is stronger inside the microcoil than that outside the microcoil, it took more time for the microrobot to traverse the trajectory along diagonal equilibrium points, as shown in Fig. 10(c) and (d). To further verify the flexible actuation of the system, the

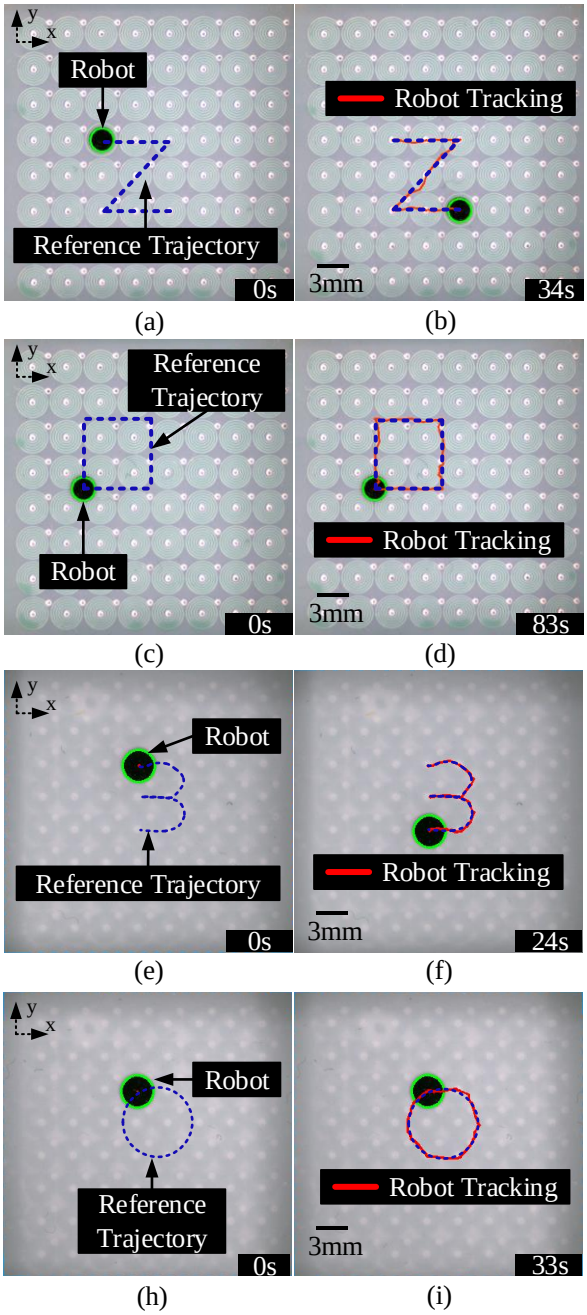

Fig. 10. Motion control of a single disc magnetic microrobot moving along prescribed waypoints. (a) and (b) Path of a single microrobot (2.5 mm diameter, 0.5 mm thick) moving in a Z-shaped trajectory. (c) and (d) Path of a single microrobot (2.5 mm diameter, 0.5 mm thick) moving in a square trajectory. (e) and (f) Path of a single microrobot (3 mm diameter, 0.5 mm thick) moving in a 3-shaped trajectory. (h) and (i) Path of a single microrobot (3 mm diameter, 0.5 mm thick) moving in a circle trajectory.

microrobot was controlled to move along a 3-shaped path， as shown in Fig. 10(e) and (f). Fig. 10(h) and (i) demonstrates the experiment of tracking circular trajectory. Then, the tracking error of the microrobot moving along different given paths is shown in Fig. 11. Especially, the error range, the mean error, and the root mean square error (RMSE) of each movement trajectory are listed in Table I. It is obvious that the maximum error range is -0.380 mm to 0.444 mm, the maximum mean error is -0.094 mm, and the maximum RMSE is 0.157 mm.

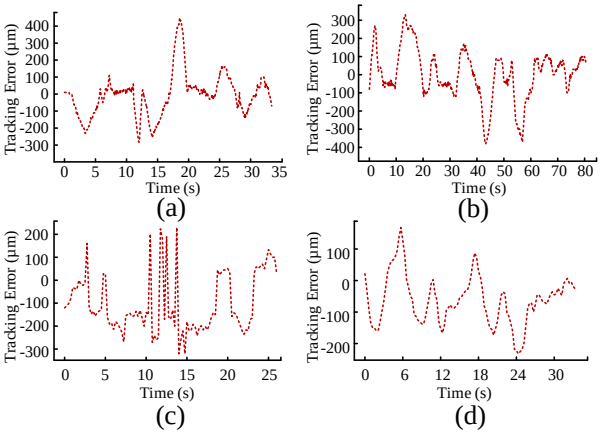

Fig. 11. Tracking error of a single microrobot moving along prescribed paths. (a) Tracking error along Z-shaped trajectory. (b) Tracking error along square trajectory. (c) Tracking error along 3-shaped trajectory. (d) Tracking error along circular trajectory.

TABLE I
TRACKING ERROR OF A SINGLE MICROROBOT

	Error Range (mm)	Mean Error (mm)	RMSE (mm)
Z-shaped	-0.283~0.444	-0.027	0.129
Square	-0.380~0.330	0.053	0.138
3-shaped	-0.325~0.234	-0.073	0.157
Circle	-0.226~0.178	-0.094	0.152

C. Multi-Robot Navigation Experiments

To show the ability of the microcoil platform for independent control of multiple microrobots, two and three microrobots motion control experiments were conducted separately in the workspace. The type of microrobots used in the experiments is the same as before, and their surfaces were dyed for the purpose of distinguishing them. Fig. 12(a) and (b) demonstrate the independent control of two microrobots. The two Z-shaped reference trajectories were provided by the user, and then two microrobots moved along their respective reference trajectories in 40 seconds. Limited by the mutual interaction force between microrobots, three microrobots can only move at the edge of the workspace, as shown in Fig. 12(c) and (d). To reduce the influence of mutual interaction force on the motion, three microrobots were forced to move between the central equilibrium point and diagonal equilibrium point, and finally reached the target position along the reference trajectories. The tracking error of two and three microrobots are separately shown in Fig. 13(a) and (b). The results show that the maximum error range is -0.25 mm to 0.35 mm, which means accurate and independent control of multiple mobile microrobots can be realized.

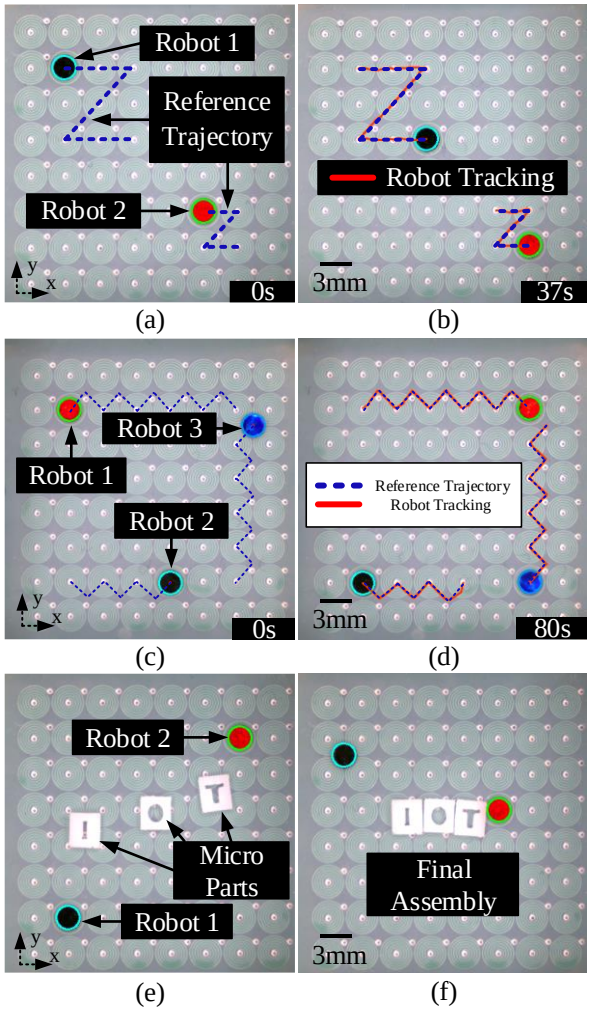

Fig. 12. Independent control of multiple microrobots moving along prescribed waypoints, respectively. (a) and (b) Two microrobots are independently actuated to move along the Z-shaped reference trajectories. (c) and (d) Motion control of three microrobots moving along their reference trajectories. (e) and (f) Assembled “IOT” structure formed by pushing the parts from their initial position (e) to final position (f) using two microrobots.

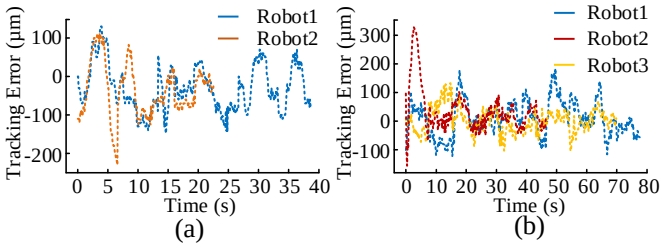

Fig. 13. Tracking errors of multiple microrobots moving along prescribed paths. (a) Tracking error of two microrobots. (b) Tracking error of three microrobots.

D. Microassembly Experiments

Microassembly experiments taking advantage of the new structure of microcoils were conducted to validate the potential of the microcoil platform to perform micromanipulation tasks. The micro parts used in the experiments were made of 3D printed resin materials. Each of them is a cuboid with the size of

$3 \times 3 \times 1$ mm. As shown in Fig. 12(e) and (f), the objective was to move the parts from an initial position [Fig. 12(e)] to a final position [Fig. 12(f)]. The waypoints of the microrobots were generated manually to ensure that the microrobots pushed the object correctly and reached the goal state. Finally, two microrobots completed the micro-assembly task.

E. Discussion

The microrobots sometimes deviate from their reference trajectories during the experiment. Even under the same input, the microrobots will respond differently to the magnetic field generated by the microcoils. On the one hand, it is because of the limitations of PCB manufacturing, small differences between the microcoils will cause errors, and the underlying current traces and vias will also affect the magnetic field in the workspace. On the other hand, it is assumed that the magnetization direction of the microrobot passes through the center of the microrobot in the analysis, but in actuality, the magnetization direction of the microrobot may be offset. Finally, the magnitude of the currents through microcoils is controlled by the PWM driver chip, which will generate current pulsation and then contribute to the magnetic field pulsation, which is also one of the reasons. However, the tracking error of the microrobot is kept between -0.380 mm to 0.444 mm. This precision maybe enough for some micro fluid based application, such as separation of droplets, transport of droplets, and mixing of droplets.

V. Conclusion and Future Work

In this study, a new local magnetic field generation system for independent control of multiple microrobots is designed, simulated, developed, and experimentally validated. The distribution of magnetic field in the workspace generated by the microcoils is researched based on an analytical model which is validated through the finite element simulation. An actuation and control method of coil array for microrobots is proposed based on the newly designed system. By the newly designed microcoil platform, the microrobot can move between any equilibrium points with the tracking error within 0.444mm. The single-robot, multi-robot navigation, and microassembly experiments are conducted by constructing an experimental platform. The experimental results show that the newly designed system can improve the capability of performing micromanipulation tasks.

In future work, improving the resolution of the coil array or designing new coil array structure may be helpful to continuous motion at any point on a plane. Path planning of multiple microrobots under constraints to find optimal trajectories is also the area of future work, which is an important step for realizing micromanipulations automatically. In addition, flexible PCB technology may be used to achieve some more complex curve surface movements.

VI. References

[1] S. Chowdhury, W. Jing, and D. J. Cappelleri, "Controlling multiple mi-crorobots: recent progress and future challenges," *J. Micro-Bio Robot.*, vol. 10, no. 1-4, pp. 1-11, Oct. 2015.

[2] S. Lee *et al.*, "A capsule-type microrobot with pick-and-drop motion for targeted drug and cell delivery," *Adv. Healthcare Mater.*, vol. 7, no. 9, p. e1700985, Feb. 2018.

[3] J. Rahmer, C. Stehning, and B. Gleich, "Remote magnetic actuation using a clinical scale system," *PLoS One*, vol. 13, no. 3, pp. 1-19, Jan. 2018.

[4] M. Sitti *et al*., "Biomedical Applications of Untethered Mobile Milli/Microrobots," *Proc. IEEE*, vol. 103, no. 2, pp. 205-224, Feb. 2015.

[5] T. Xu, W. Gao, L. -P. Xu, X. Zhang, and S. Wang, "Fuel-free synthetic micro-/nanomachines," *Adv. Mater.*, vol. 29, no. 9, p. 1603250, Mar. 2017.

[6] I. Grexa *et al*., "Single-cell elasticity measurement with an optically actuated microrobot," *Micromachines*, vol. 11, no. 9, p. E882, Sep. 2020.

[7] J. Park *et al*., "Acoustically mediated controlled drug release and targeted therapy with degradable 3D porous magnetic microrobots," *Adv. Healthcare Mater.*, vol. 10, no. 2, pp. e2001096, Jan. 2021.

[8] Y. S. Kochergin *et al*., "Hybrid inorganic-organic visible-light-driven microrobots based on donor-acceptor organic polymer for degradation of toxic psychoactive substances," *ACS nano*, vol. 15, no. 11, pp. 18458-18468, Nov. 2021.

[9] Franco N. Piñan Basualdo *et al*., "A microrobotic platform actuated by thermocapillary flows for manipulation at the air-water interface," *Science robotics*, vol. 6, no. 52, p. eabd3557, Mar 2021.

[10] E. Diller, J. Giltinan, G. Z. Lum, Z. Ye, and M. Sitti, "Six-degree-of-freedom magnetic actuation for wireless microrobotics," *Int. J. Robot. Res.*, vol. 35, no. 1-3, pp. 114-128, Jan. 2016.

[11] T. Xu, J. Yu, X. Yan, H. Choi, and L. Zhang, "Magnetic actuation based motion control for microrobots: An overview," *Micromachines*, vol. 6, no. 9, pp. 1346–1364, Sep. 2015.

[12] X. Zhang, H. Kim, and M. J. Kim, "Design, implementation, and analysis of a 3-D magnetic tweezer system with high magnetic field gradient," *IEEE Trans. Instrum. Meas.*, vol. 68, no. 3, pp. 680–687, Mar. 2019.

[13] D. Li, F. Niu, J. Li, X. Li, and D. Sun, "Gradient-enhanced electromagnetic actuation system with a new core shape design for microrobot manipulation," *IEEE Trans. Ind. Electron.*, vol. 67, no. 6, pp. 4700–4710, Jun. 2020.

[14] H. Nourmohammadi, J. Keighobadi, and M. Bahrami, "Design, dynamic modelling and control of a bio-inspired helical swimming microrobot with three-dimensional manoeuvring," *Trans. Inst. Meas. Control*, vol. 39, no. 7, pp. 1037–1046, Jul. 2017.

[15] Q. Fan, P. Zhang, J. Qu, W. Huang, X. Liu and L. Xie, "Dynamic magnetic field generation with high accuracy modeling applied to magnetic robots," *IEEE Trans. Magn.*, vol. 57, no. 7, pp. 1-10, July 2021.

[16] E. B. Steager, M. S. Sakar, C. Magee, M. Kennedy, A. Cowley, and V. Kumar, "Automated biomanipulation of single cells using magnetic microrobots," *Int. J. Robot. Res.*, vol. 32, no. 3, pp. 346-359, Mar. 2013.

[17] M. Guix, J. Wang, Z. An, G. Adam, and D. J. Cappelleri, "Real-time force-feedback micromanipulation using mobile microrobots with colored fiducials," *IEEE Robot. Autom. Lett.*, vol. 3, no. 4, pp. 3591-3597, Oct. 2018.

[18] Y. Gao, F. Wei, Y. Chao, and L. Yao, "Bioinspired soft microrobots actuated by magnetic field," *Biomed Microdevices*, vol. 23, no. 4, p. 52, Oct. 2021.

[19] M. Salehizadeh and E. Diller, "Three Dimensional Independent Control of Multiple Magnetic Microrobots via Inter-Agent Forces," *International Journal of Robotics Research*, vol. 39, no. 12, pp. 1377-1396, 2021.

[20] I. S. M. Khalil *et al*., "Independent actuation of two-tailed microrobots," *IEEE Robot. Automat. Lett.*, vol. 3, no. 3, pp. 1703-1710, Jul. 2018.

[21] A. Becker et al., "Massive uniform manipulation: Controlling large populations of simple robots with a common input signal," *Proc. IEEE/RSJ Int. Conf. Intell. Robots Syst.*, pp. 520–527, 2013.

[22] S. E. Chung, X. Dong, and M. Sitti, "Three-dimensional heterogeneous assembly of coded microgels using an untethered mobile microgripper," *Lab Chip*, vol. 15, no. 7, pp. 1667–1676, Jul. 2015.

[23] F. Ongaro, S. Pane, S. Scheggi and S. Misra, "Design of an electromagnetic setup for independent three-dimensional control of pairs of identical and nonidentical microrobots," *IEEE Trans. Robot.*, vol. 35, no. 1, pp. 174-183, Feb. 2019.

[24] S. Chowdhury, B. V. Johnson, W. Jing, and D. J. Cappelleri, "Designing local magnetic fields and path planning for independent actuation of multiple mobile microrobots," *J. Micro-Bio Robot.*, vol. 12, no. 1, pp. 21–31, Jun. 2017.

[25] B. V. Johnson, S. Chowdhury, and D. Cappelleri, "Local magnetic field design and characterization for independent closed-loop control of

multiple mobile microrobots," *IEEE/ASME Trans. Mechatronics*, vol. 25, no. 2, pp. 526–534, Apr. 2020.
[26] S. Chowdhury, W. Jing, and D. J. Cappelleri, "Towards independent control of multiple magnetic mobile microrobots," *Micromachines*, vol. 7, no. 1, pp. 1-14, Dec. 2016.
[27] Y. Kantaros, B. V. Johnson, S. Chowdhury, D. J. Cappelleri, and M. M. Zavlanos, "Control of magnetic microrobot teams for temporal micromanipulation tasks," *IEEE Trans. Robot.*, vol. 34, no. 6, pp. 1472–1489, Dec. 2018.
[28] Q. Xu, Q. Hu, H. Wang, Z. -H. Mao and M. Sun, "Optimal design of planar spiral coil for uniform magnetic field to wirelessly power position-free targets," *IEEE Trans. Magn.*, vol. 57, no. 2, pp. 1-9, Feb. 2021.
[29] D. E. Gray, *American Institute of Physics (AIP)*. Handbook. New York, NY, USA: McGraw-Hill, 1972.

Guangming Cui received the B.Sc. degree in 2020 from the School of Internet of Things Engineering, Jiangnan University, Wuxi, China, where he is currently working toward the M.Sc. degree in electrical engineering.

His research interests include magnetic field actuation technology and micromanipulation.

Pengsong Zhang received the bachelor's and master's degrees from the School of Internet of Things Engineering, Jiangnan University, Wuxi, China, in 2018 and 2021, respectively.

His research interests include robotics, computer vision, and biomedical technology.

Xinyu Liu (S'06-M'10) received the B.Eng. and M.Eng. degrees from the Harbin Institute of Technology, Harbin, China, in 2002 and 2004, respectively, and the Ph.D. degree from the University of Toronto, Toronto, ON, Canada, in 2009, all in mechanical engineering.

He is currently the Percy Edward Hart Professor with the Department of Mechanical and Industrial Engineering and is cross-appointed with the Institute of Biomedical Engineering, University of Toronto, ON, Canada.

Before joining the University of Toronto in September 2017, he was an Associate Professor and the Canada Research Chair in Microfluidics and BioMEMS with the Department of Mechanical Engineering, McGill University, Montreal, QC, Canada. His research interests include microrobotics, nanorobotics, soft robotics, and microfluidics.

Linbo Xie received the B.S. degree from Hunan Normal University, Changsha, China, in 1996, the M.S. degree from Southwest Jiaotong University, Chengdu, China, in 2001, and the Ph.D. degree in control theory and control engineering from Huazhong University of Science and Technology, Wuhan, China, in 2004.

He is currently with the School of Internet of Things Engineering, Jiangnan University, Wuxi, China, where he has been a full professor since 2014. His research interests include process modeling and control, intelligent detection and system safety.

Wentao Huang received the Ph.D. degree in Electrical Engineering from Southeast University, Nanjing, China, in 2020.

From January 2018 to January 2019, he was a joint Ph.D. student with the School of Electrical and Data Engineering, University of Technology Sydney, NSW, Australia. Since 2020, he has been with Jiangnan University, Wuxi, China, where he is currently a Lecturer with the School of Internet of Things Engineering. His teaching and research interests include permanent magnet machine drives, fault diagnosis and fault-tolerant control.

Peng Pan received the B.Eng. and M.Eng. degrees in mechanical engineering from the Soochow University, Suzhou, China, in 2013 and 2016, respectively. He obtained the Ph.D. degree in mechanical engineering, McGill University, Montreal, QC, Canada, in 2021.

Now he is a postdoctoral researcher in the department of Mechanical and Industrial Engineering with the University of Toronto, Toronto, ON, Canada. His research interests include automated robotic manipulation, MEMS (microelectromechanical systems), microfluidics, and large-scale gene screening.

Juntian Qu (S'15-M'20) received the B.Eng. and M.Eng. degrees in automatic control theory and engineering from Northeastern University, Shenyang, China, in 2012 and 2014, respectively, and the Ph.D. degree from McGill University, Montreal, QC, Canada, in 2019, in mechanical engineering.

He is currently the Shuimu Postdoctoral Fellow and an Assistant Research Fellow with the Department of Mechanical Engineering, Tsinghua University and the Incoming Assistant Professor with Shenzhen International Graduate School of Tsinghua University. His current research interests include SEM-based robotic micro and nano manipulation, nanomaterial characterization, MEMS and 3D printing.

Qigao Fan (Member, IEEE) received the Ph.D. degree in mechatronic engineering from the School of Mechatronic Engineering, China University of Mining Technology, Xuzhou, China, in 2013.

Since 2013, he has been with Jiangnan University, Wuxi, China, where he is currently an Associate Professor with the School of Internet of Things Engineering. From 2018 to 2019, he was a Visiting Scholar with the Department of Mechanical and Industrial Engineering, University of Toronto, Toronto, ON, Canada. His teaching and research interests include motor control, robotics, intelligent sensors, and IoT technology.